A robust method for mechanical characterization of heterogeneous materials by nanoindentation grid analysis

Cesar-Moises Sanchez-Camargo, Anis Hor, Mehdi Salem, Catherine Mabru

Materials and Design 194 (2020) 108908

Contents lists available at ScienceDirect

Materials and Design

journal homepage: www.elsevier.com/locate/matdes

A robust method for mechanical characterization of heterogeneous materials by nanoindentation grid analysis

Cesar-Moises Sanchez-Camargo, Anis Hor *, Mehdi Salem, Catherine Mabru

Institut Clément Ader (ICA), Université de Toulouse, CNRS UMR 5312-ISAE-SUPAERO-UPS-INSA-Mines Albi, 3 rue Caroline Aigle, 31400 Toulouse, France

HIGHLIGHTS

- Analysis of the nanoindentation data gathered by a grid applied on the surface of the investigated heterogeneous materials
- Detection of phases and estimation of their mechanical properties
- Phase fraction detection and estimation by different methods
- Elastoplastic characterization of the phases and the bulk material by inverse analysis coupled with finite element modeling
- Improved results against the statistical analysis using deconvolution technique

GRAPHICAL ABSTRACT

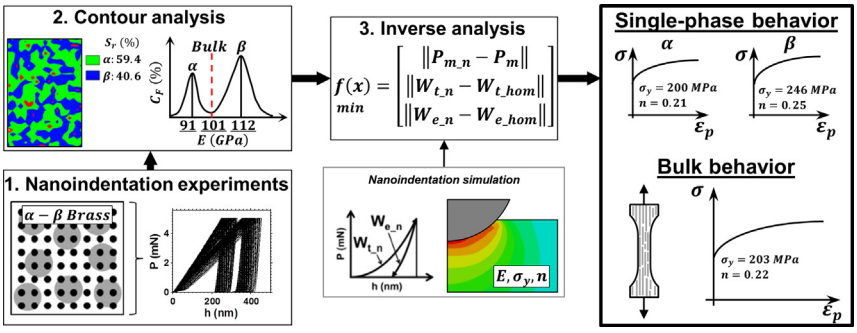

ARTICLE INFO

Article history:
Received 3 March 2020
Received in revised form 31 May 2020
Accepted 20 June 2020
Available online 25 June 2020

Keywords:
Nanoindentation
Finite element analysis
Plasticity
Composites
EBSD

ABSTRACT

The study presents the analysis of the contour plots obtained from nanoindentation grids conducted on CuZn40Pb2 brass and W-Cu, which are heterogeneous materials having different microstructure and mechanical properties. The aim is to increase the detection capacity of the mechanical properties of the phases respect to the statistical analysis, but also to propose a formulation for the inverse analysis of nanoindentation data allowing the full elastoplastic characterization. Analysis of contour plots provides curves where the mean value of the phases and the bulk value can be read directly. In complex microstructures, this gives access to the predominant mechanical properties facilitating the interpretation of the results. The estimation of the phase fractions by this proposed method is better than the estimation performed with statistical analysis. The estimation of the standard deviation is equivalent to the statistical analysis in most cases; however the difference is large on skewed distributions. The formulation of the objective function for inverse analysis is able to manage large number of indentations, producing elastoplastic parameters with excellent accuracy compared to parameters identified by tensile test.

1. Introduction

The nanoindentation test is a well-known technique used to estimate the hardness and elastic modulus. The principle of this test is to penetrate the sample surface with an indenter whose elastic modulus is several times higher than the elastic modulus of the tested material. Throughout the test, the force and the displacement on the indenter are recorded, producing the indentation curve. This indentation curve has been widely used in the literature as a means for the estimation of hardness and elasticity [1,2]. The formulations used in these estimations are based on the hypothesis of homogeneity and isotropy of the sample [3,4], therefore the stress and strain are independent of the indentation depth. Constantinides et al. [5] took advantage of the high precision of

* Corresponding author.
E-mail address: anis.hor@isae-supaero.fr (A. Hor).

https://doi.org/10.1016/j.matdes.2020.108908
0264-1275/

the nanoindentation test to evaluate the mechanical properties of the different phases of heterogeneous materials. The principle of their method consists in the use of a large nanoindentation grid over a representative surface coupled with a statistical analysis of the nanoindentation data. Thus the phase fraction, the mean and the standard deviation of the mechanical properties corresponding to each phase can be estimated.

The nanoindentation grid must respect three important aspects:

i. The indentation depth, h, must be shallow enough to measure only the properties of each phase, i.e. at most $h < 0.1D$, where D is the characteristic diameter of the phase.
ii. The size of the nanoindentation grid must satisfy $d_i\sqrt{N} \gg D$, where N is the total number of indentations in the grid.
iii. The distance, d_i, between indentations must be three times the size of the residual imprint to avoid interferences between tests [6].

The statistical analysis was based on the deconvolution of mechanical response distributions assumed to be Gaussian distributions. The mechanical property x of each phase J can be approximated by:

$$p_J(x) = \frac{1}{\sqrt{2\pi s_J^2}} exp\left(-\frac{\left(x-\mu_J\right)^2}{2s_J^2}\right) \quad (1)$$

where μ_J and s_J are the mean and the standard deviation of the N_J values respectively, calculated from:

$$\mu_J = \frac{1}{N_J}\sum_{k=1}^{N_J} x_k ; s_J^2 = \frac{1}{N_J - 1}\sum_{k=1}^{N_J}\left(x_k - \mu_J\right)^2 \quad (2)$$

The mechanical property x obeys the density function:

$$P(x) = \sum_{J=1}^{m} f_J p_J(x) \quad (3)$$

where f_J is the phase fraction of the phase J, subject to the constraint:

$$\sum_{J=1}^{m} f_J = 1 \quad (4)$$

The problem is solved by minimizing:

$$min \sum_{i=1}^{t} \frac{(P_i - P(x_i))^2}{t} \quad (5)$$

where P_i corresponds to the distribution of the experimental nanoindentation and t is the chosen number of bins for the histogram.

Later, using this technique, several authors [7,8] have analyzed several heterogeneous materials ranging from simple to complex microstructures to evaluate the accuracy of the method. They found that small phase fractions can be hidden by other phases, making it difficult to detect them accurately [9]. The nanoindentation grid data is also used to build maps of the mechanical properties on the sample surface [10–12]. The principle of such mappings is to link the surface coordinates of each indentation to the value of the measured mechanical property. Then the contour lines defining regions on the plot sharing the same value are built using interpolation techniques [13–15]. The precision of this method is debatable especially when the phases present in the material have similar properties or the proportions between these phases are very different.

The objective of this paper is to propose a new more accurate method to analyze the nanoindentation data gathered by nanoindentation grid of heterogeneous material. The principle of this method relies on the analysis of the nanoindentation grid contour plot to obtain the mean, the standard deviation and the phase fraction of the mechanical properties associated to each phase. On the other hand, a new formulation of the objective function for the inverse analysis, allowing the use of the nanoindentation data obtained by contour analysis, is proposed.

A comparison between this proposed method and the statistical method presented above will be performed to prove that the proposed method is capable of providing a more efficient identification of the mechanical properties compared to the statistical method. This method will provide tools for better interpretation of the nanoindentation results. Finally, the results of the reverse analysis will be validated by the macroscopic behavior.

2. Experimental and computational considerations

2.1. Microstructural characteristics of investigated materials

To validate this new method, two materials were selected; the first material is forged biphasic brass (CuZn40Pb2) having two phases: α and β' (Fig. 1a) with very close mechanical properties. The second material is W-Cu elaborated from powder metallurgy by Spark Plasma Sintering (SPS) process and having Cu and W phases (Fig. 1b) with very different mechanical properties [16]. This choice will therefore validate the method with two extreme cases. The microstructures of these two materials are presented in Fig. 1.

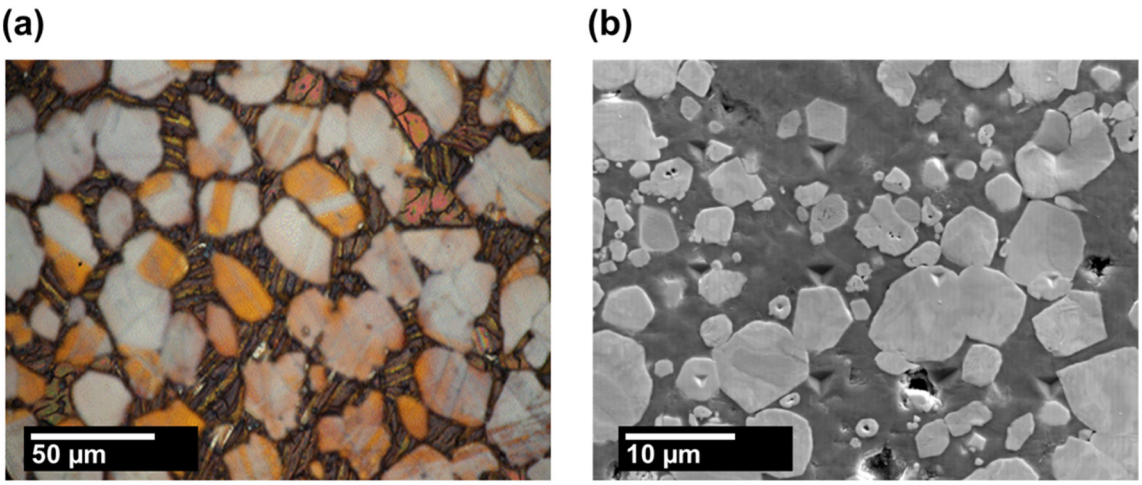

Fig. 1. Microstructure of (a) CuZn40Pb2 brass and (b) W-Cu materials.

The EBSD analysis allowed the microstructural-crystallographic characterization as well as the determination of the phase fractions present in each material. The EBSD data was treated and analyzed using the MTEX toolbox [17]. On CuZn40Pb2 brass, the measurements revealed a clean and non-textured surface (Fig. 2a1). The measured phase fractions were $\alpha = 62.72\%$, $\beta' = 33.03\%$ (Fig. 2b1), and zero solution (non-indexed) 4.25%. A misorientation of 6° was detected in some regions of the phase β (Fig. 2c1). Since the EBSD observations revealed a well-defined microstructure, free of deformation and hardening, it was considered that this surface was convenient for the inverse nanoindentation analysis. On the W-Cu material, the analysis revealed a fine microstructure (Fig. 2a2). The phase fractions were 41.29% for the Cu, 40.1% for the W, and 18.61% for the zero solution (Fig. 2b2). The misorientation reached until 60° in some regions (Fig. 2c2).

Table 1 summarizes the results of this EBSD analysis before and after correction of the results. The correction consists in deleting the non-indexed regions and assigning them one of the two phases based on the neighboring zones. This method is often used in EBSD analysis when the indexing rate is less than 100%.

The diameter of the grains, which corresponds to the greatest distance between any two vertices of the grain boundary [18], was computed for both materials (Fig. 3). The mean grain diameter was estimated:

- at 17 μm for α phase and 24, 8 μm for β' phase in the case of CuZn40Pb2 brass.
- at 6 μm for W phase and 5.6 μm for Cu phase in the case of W-Cu alloy.

2.2. Uniaxial tensile behavior

The macroscopic mechanical behavior of the biphasic CuZn40Pb2 brass was characterized by uniaxial tensile test (Fig. 4). The tensile experiments were conducted on samples were the loading axis was parallel to the *RD*. The W-Cu was not characterized by tensile test due to the limited quantity of material elaborated by SPS process.

The Young's modulus, *E*, was estimated from the conventional definition [19]. The zero-offset plastic strain was fitted through least squares method according to the elastoplastic power law [20]:

$$\sigma = \sigma_y\left(1 + \frac{E}{\sigma_y}\varepsilon_p\right)^n \tag{6}$$

where, σ_y represents the yield strength and *n* denotes the hardening exponent. The yield strength was taken from the experimental curve and not from the fitting value of σ_y on Eq. (6). The values of the elastoplastic parameters were defined as reference to evaluate the performance of the inverse analysis.

2.3. Nanoindentation experiments

The Berkovich indenter is widely used to conduct nanoindentation experiments. However it has an inconvenient: the wear on the tip, which is a physical characteristic and cannot taking account by any model, as explained by Pelletier et al. [21].

In previous studies conducted on 316L (a single phase austenitic stainless steel), we found that at the indentation depth of the study presented in this paper ($h_m \approx 200$ nm), the parameter identification of the constitutive equation is not well achieved when using a Berkovich indenter due to tip defects [22,23]. The literature suggests that small variations in the tip induce large variations in the nanoindentation curve [20], which is shown in Fig. 5a.

In contrast, the spherical indenter obtained better results (Fig. 5b). A particular interest of this research paper is to provide a way to perform a parameter identification of the constitutive equation of the material; therefore the spherical indenter was selected.

It is well known that spherical indenters are particularly interesting in parameter identification because they are able to produce different values of strain in function of the indentation depth [24]. However since the proposed method consists of a large number of indentations (800 in about 55 h), this inherent characteristic of spherical indenters has been neglected in this paper and all the experiments were conducted at a single indentation load as detailed below.

The nanoindentation samples were the same used for the EBSD measurements. The surface has been prepared as described in [22]. The nanoindenter used in the experiments was a NHT2 from Anton-Paar, equipped with a diamond spherical indenter with a radius of 2 μm. The nanoindentation experiments were conducted in load control with a peak load $P_m = 5$ mN at loading/unloading rate of 5 mN/min with 10 s of holding at peak load. A grid of 20×40 nanoindentations separated by 10 μm in both directions was performed on both samples to cover a surface of 190×390 μm by a total of 800 nanoindentations.

The elastic modulus of the CuZn40Pb2 brass and the W-Cu alloy, were estimated through the method of Oliver and Pharr [1,2] using the function area:

$$A = \pi\left(2Rh_c - h_c^2\right) \tag{7}$$

where *A* is the projected contact area, *R* is the indenter radius and h_c is the contact depth. The elastic modulus is computed from the equation:

$$S = \frac{2}{\sqrt{\pi}}E_r\sqrt{A} \tag{8}$$

where $S = dP/dh$ is the contact stiffness and E_r is the effective elastic modulus defined by the equation:

$$\frac{1}{E_r} = \frac{1-\nu^2}{E} + \frac{1-\nu_i^2}{E_i} \tag{9}$$

where *E* and *ν* are the elastic constants of the sample, and E_i and ν_i are the elastics constants of the indenter.

The hardness was computed from the equation:

$$H = \frac{P_m}{A} \tag{10}$$

The maximum indentation depth, h_m, the total indentation work W_t, and the elastic indentation work, W_e, were obtained directly from the nanoindentation force-displacement (P,h) diagram composed by the loading curve from $(P = 0, h = 0)$ to $(P = P_m, h = h_m)$ and the unloading curve from $(P = P_m, h = h_m)$ to $(P = 0, h = h_f)$. The total indentation work was computed from the loading curve through:

$$W_t = \int_0^{h_m} Pdh \tag{11}$$

and the elastic indentation work was determined from the unloading curve through:

$$W_e = \int_{h_f}^{h_m} Pdh \tag{12}$$

The value of the total work quantity is potentially affected by the pop-in events. For the two studied materials, pop-in events were observed at the beginning of the loading branch of several nanoindentation curves (Fig. 5). However, excluding the pop-in portion in the loading curve introduces a variation of 3% in this variable. Therefore, to simplify the experimental data analysis, the effect of pop-in events on the indentation total work was neglected and this quantity was calculated from the full loading data.

The indentation works, W_e and W_t are presented in this study because they will be used later in the formulation of the objective function

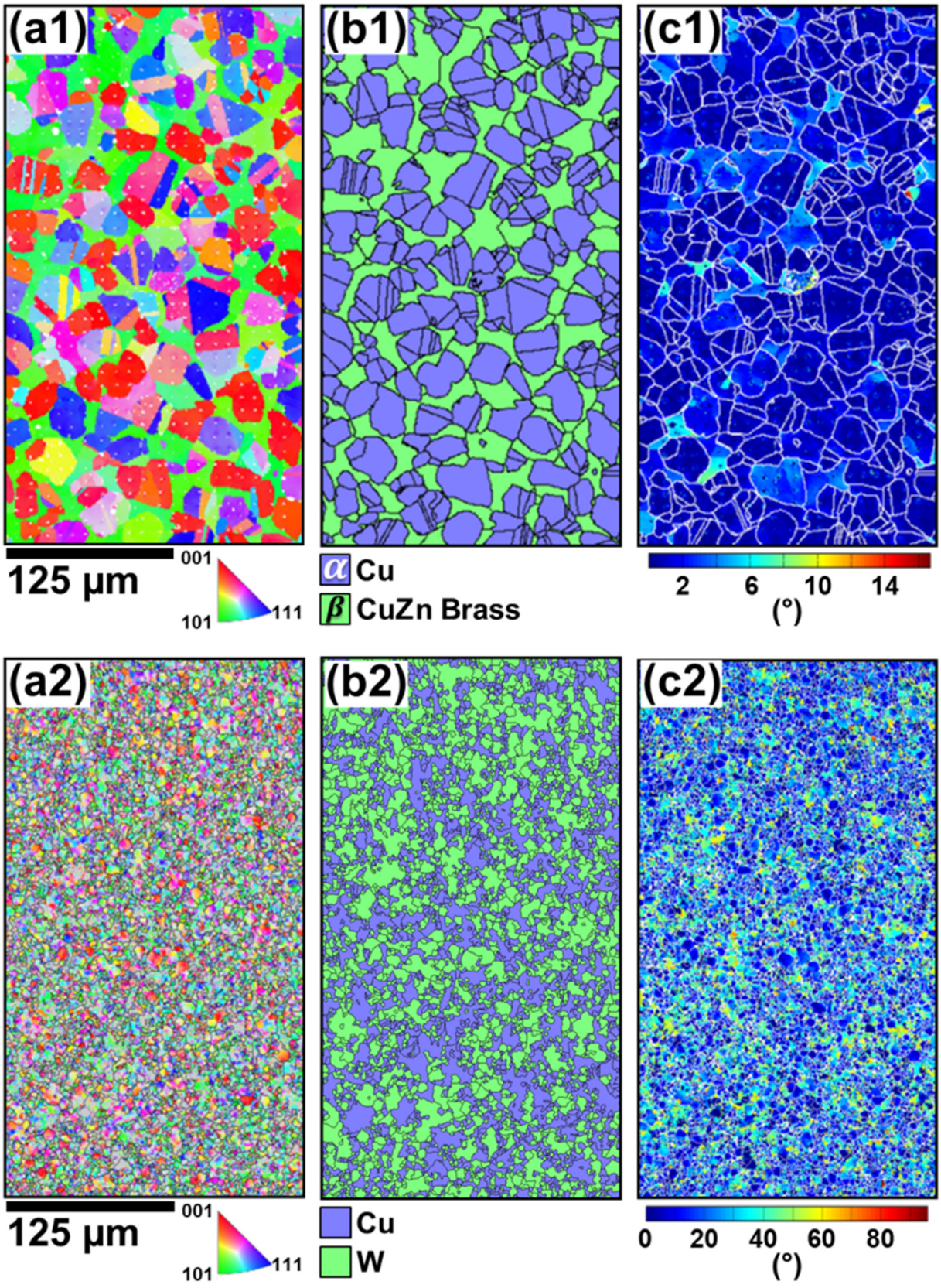

Fig. 2. EBSD microstructural analysis of (1) CuZn40Pb2 brass and (2) W-Cu materials: (a) mean orientation map, (b) phase map and (c) misorientation map.

Table 1
Nature and fraction of phases present in the two materials obtained by EBSD.

Material	Phases	Crystal structure	Phase fraction (EBSD)	Phase fraction (EBSD) after correction
CuZn40Pb2 brass	α	FCC	62,7%	70%
	β'	BCC	33%	30%
	Non indexed	–	4,3%	
W-Cu	Cu	FCC	41,3%	50%
	W	BCC	40,1%	50%
	Non indexed	–	19,2%	

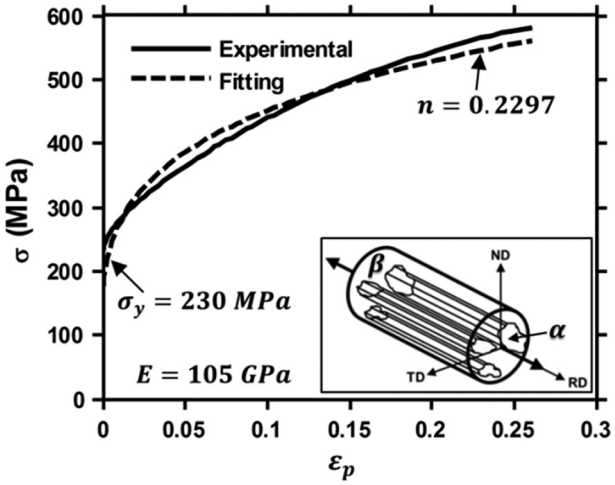

Fig. 4. True stress-true strain curve and elastoplastic parameters of CuZn40Pb2 brass.

necessary for the elastoplastic behavior identification. Indeed, these two variables allow the use of an efficient energy or integral formulation in optimization problems. In addition, these two variables make it possible to take into account the entire loading-unloading curve [22,23].

The contour plots of these different quantities are illustrated for both materials in Fig. 6. As can be seen, these maps cannot be explored directly to determine the mechanical properties of each phase and require an analysis method.

2.4. Contour lines analysis of the nanoindentation data

Several methods can be used to treat statistically the nanoindentation data, e.g. clustering methods such as support vector machines (SVM) and artificial neural networks (ANN) [24]. These methods are mainly used to statistically process large databases. The convergence of these methods strongly depends on the size of this database. These methods have not been used in the literature to characterize the heterogeneous materials by nanoindentation because actually the nanoindentation test remains a time consuming test and also large indentation matrix could affect the tip geometry deviating the results. Then, the objective of this study is to provide a simple and robust method for

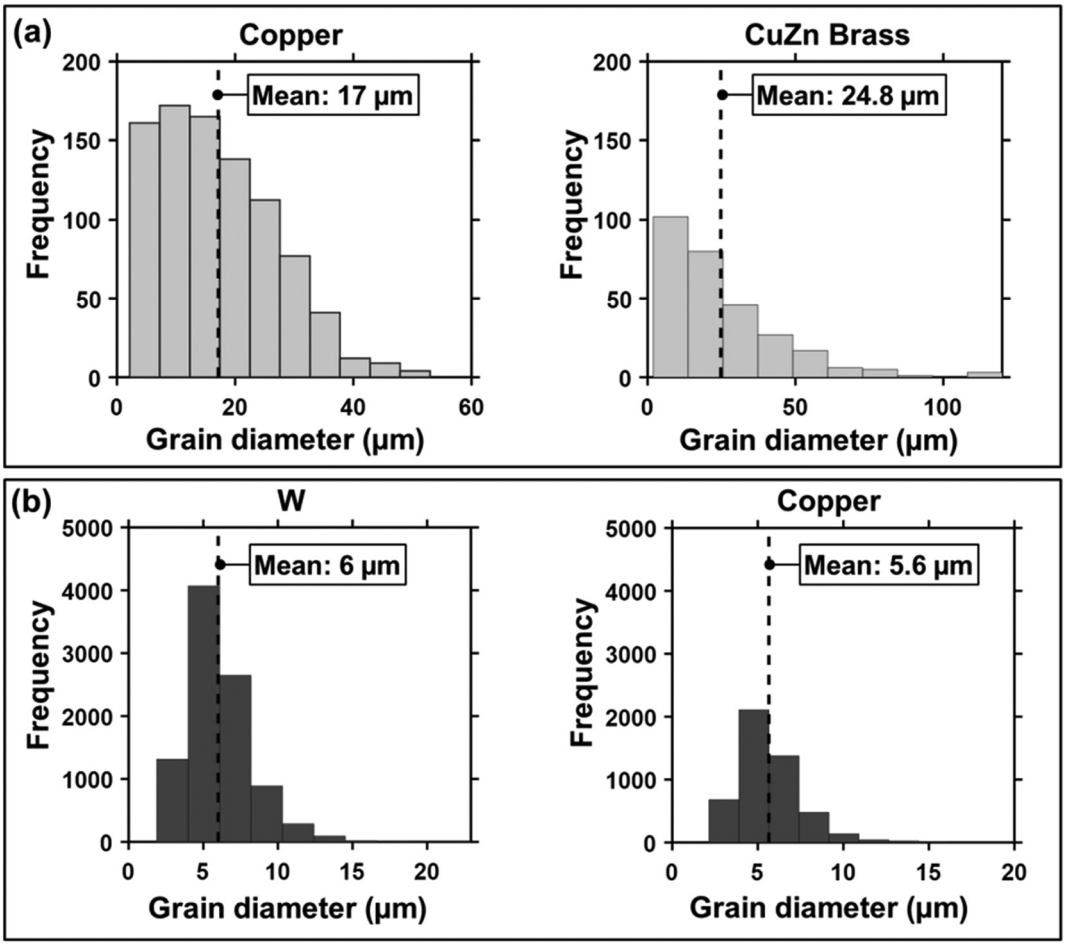

Fig. 3. Distribution of the diameter grain size of each phase for: (a) CuZn40Pb2 brass and (b) W-Cu.

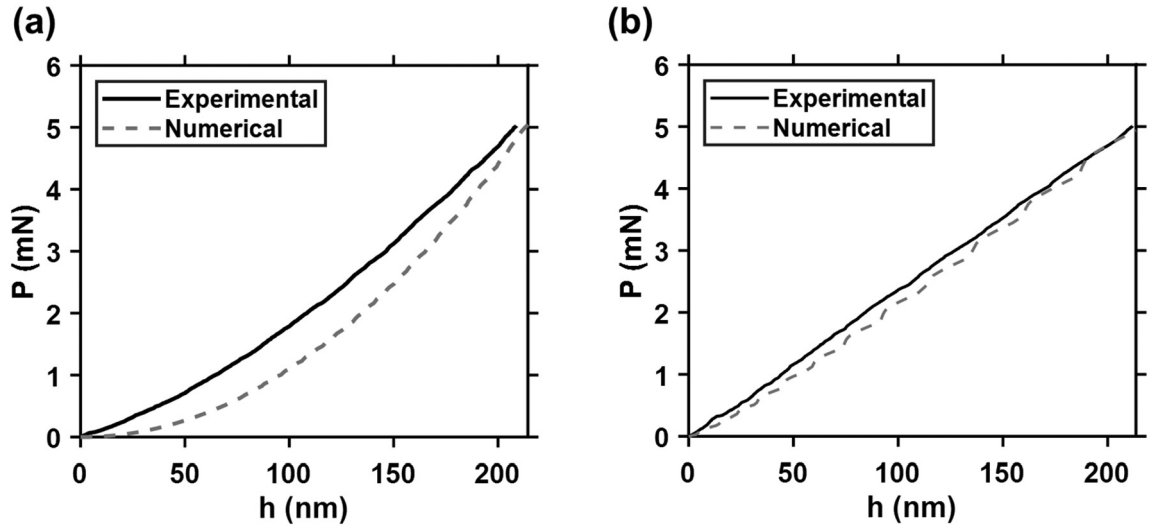

Fig. 5. Comparison of nanoindentation simulations versus experiments with applied load of $P_m = 5$ mN, conducted with (a) Berkovich indenter and (b) Spherical indenter of a radius of 2 μm.

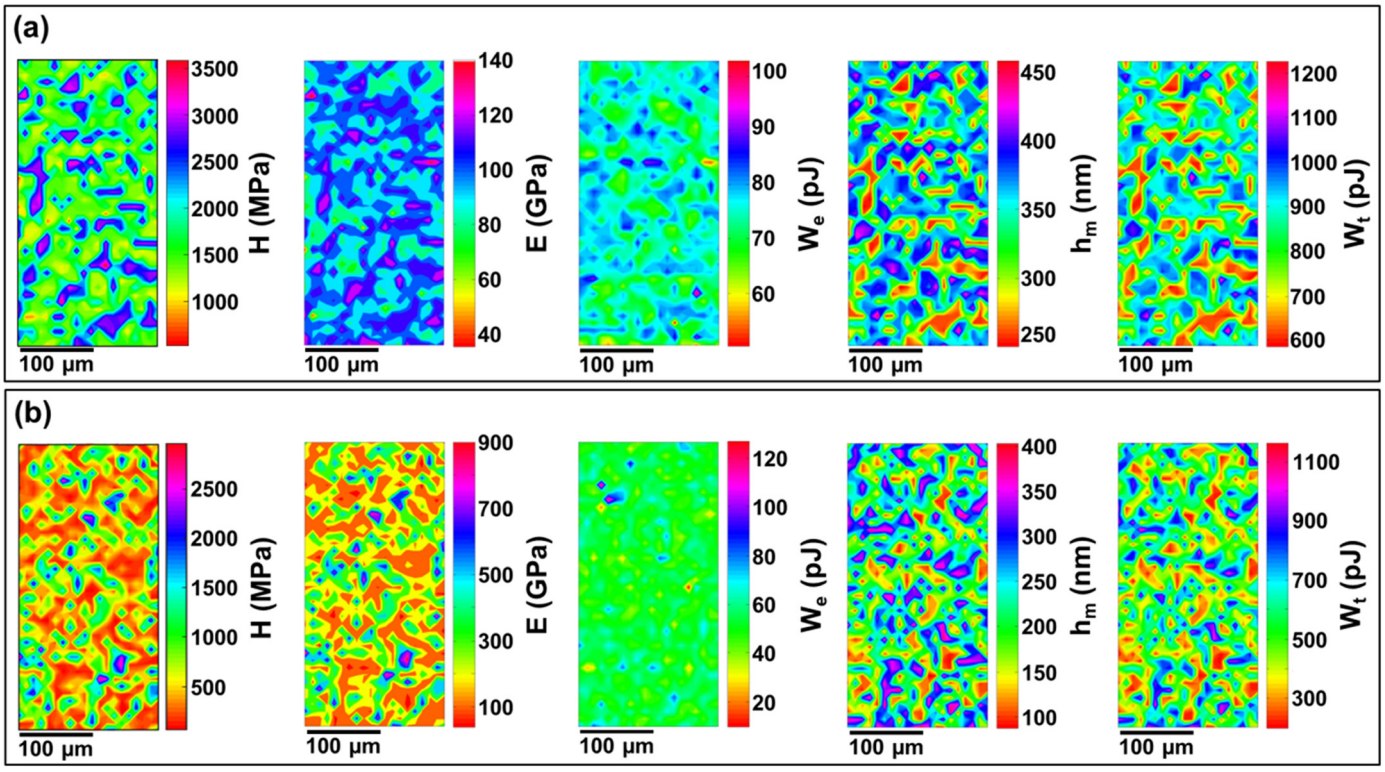

Fig. 6. Contour plots of the nanoindentation quantities: (a) for CuZn40Pb2 brass and (b) for W-Cu.

determining the two or more phase's properties of heterogeneous material from a reasonable amount of tests (e.g. 800 indents in 55 h).

Contour plot methods are widely used in science and engineering to facilitate the interpretation of data gathered experimentally or numerically. This kind of plots allows the visualization of three-dimensional data in two-dimensional plots (Fig. 7(a) and (b)) [24,25]. But also contour plots are able to represent the distribution of a given data set over a region, e.g. the stress distribution from results of Finite Element Simulations, where the data set is represented over the model geometry (Fig. 7 (c)). Visualization of three-dimensional data in two-dimensional plots can be achieved by distributing the data along z — *axis* (Fig. 7(a)) into equally spaced subintervals, and assigning a color to each subinterval (color bar in Fig. 7(b)). The colors are then mapped over the two-dimensional plot to indicate the values at each location (Fig. 7 (b) includes the colors of the contours and its level values). For this reason contour plots are also known as iso-contour, iso-line or iso-value plots.

Contour plots can be generated from regular or irregular grids distributed on a plane. A contour plot using a regular grid on x-y plane is shown in Fig. 7(b). However in Finite Element, the contour plot is generated from a mesh where the elements and nodes have an irregular distribution in most cases. The methods and conventions used to

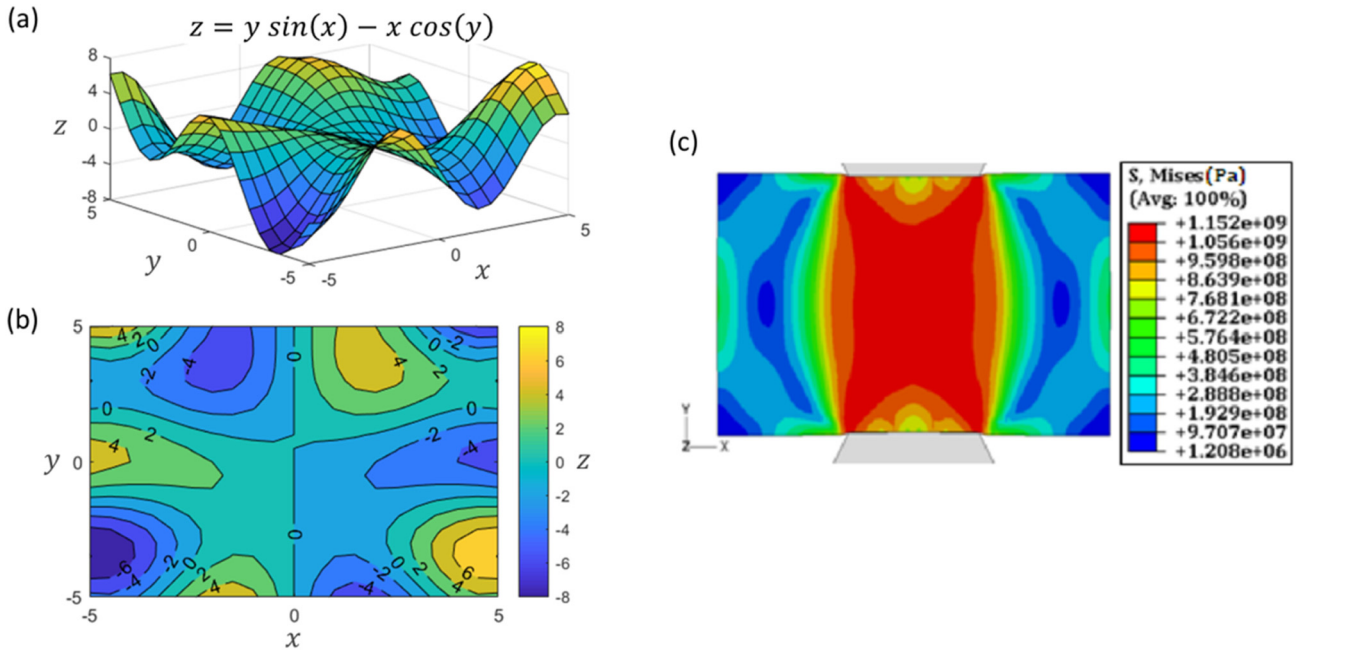

Fig. 7. Use of contour plots: to represent the three-dimensional data in (a) in two-dimensional contour plot in (b), and in (c) to represent the von-Mises stress distribution over FE geometry.

generate the contour plots are out of the scope of this paper and in general depend on the software used to generate such plots (e.g. Matlab, Python, etc.; please refer to its corresponding user manual).

Regardless of the software used to create contour plots, the users usually can access the two basic data sets generated with a contour plot function: 1) a vector containing the values linked to each color (levels) and 2) the matrix containing the vertices defining each contour for a given level; from the vertices are generated the lines enclosing a surface which is filled with the color associated to its level. These two data sets can be analyzed with the method described below to assess the mechanical properties of multiphase materials and its corresponding phase-fractions.

The method proposed to analyze the contour plots is summarized in the algorithm shown in Fig. 8. This algorithm is used to analyze each indentation quantity (E, H, W_t, …). Its implementation in Matlab is detailed later. To implement the algorithm in other software, please refer to the corresponding manual to get access to the required data sets obtained from a contour plot function.

In general, a contour plot takes as inputs the nanoindentation data (which includes the surface coordinates of the tests and its associated nanoindentation values) and the number of levels in which the range of the nanoindentation value will be divided. In this case the number of levels is analog to the number of bins used to create a histogram.

The function returns the set of levels and subsets of vertices associated to each level. The vertices are used to plot the contour lines. The contour lines enclose the area filled with the color associated with a given level, allowing the construction of every single contour patch in the plot.

Then, the number of lines associated with each level is represented as a percent of the total number of lines generated by the contour function (contour fractions). The levels corresponding to the dominant mechanical properties will concentrate the maximum quantity of contour lines, revealing the mean value of the mechanical property associated with each phase. This procedure is analog to statistical methods that group the data to identify the mean values of multi-modal data. The mean values extracted from quantities related to the nanoindentation curve (h_m, W_t and W_e in this study) are used to estimate the plastic properties of the fractions and the bulk by inverse analysis as explained in the Section 2.5. Finally, the areas of the contours corresponding to the peak levels are calculated to estimate the phase fractions present in the studied material.

In this study, nanoindentation grid conducted on the surface of a sample was a regular grid. The contour plots used in this study were generated in Matlab, using the built-in function “contour”. The contour function in MATLAB picks the levels by dividing the data into equally spaced intervals for the chosen number of contours and interpolates and smooths the data. This method is well suited to the problem of nanoindentation of a multiphase material because it smooths the errors caused by the indentations located at the interface between two phases

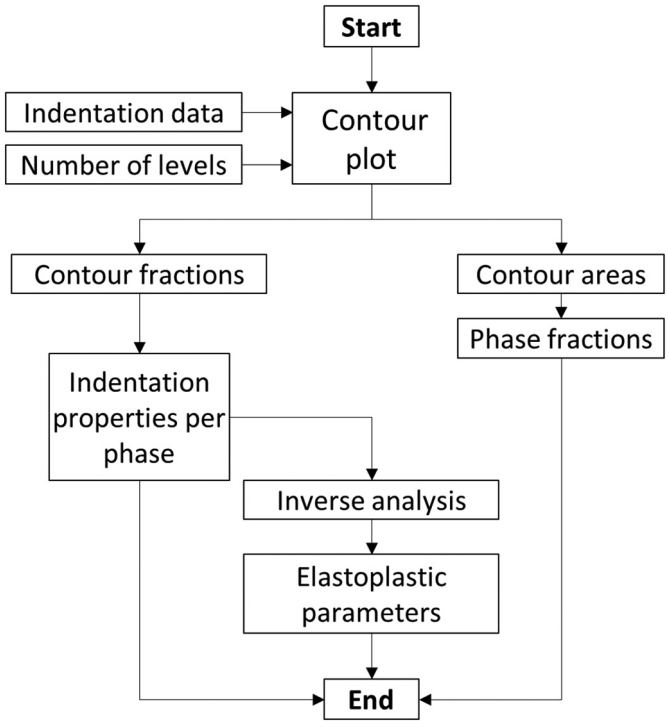

Fig. 8. Algorithm used to analyze the data generated by a contour plot software.

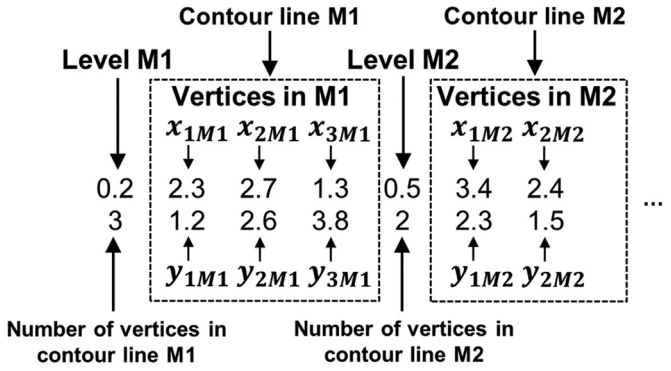

Fig. 9. Example of the contour matrix architecture.

of very different hardness. The smoothing applied by the method makes it possible to reduce the noise caused by these indentations and the properties of each phase can be observed statistically.

The inputs of the contour function are: a) the (x,y) coordinates of the nanoindentation points, b) the values of a nanoindentation quantity associated to each (x,y) point and c) the number of levels in which the nanoindentation data will be distributed. The function returns the "contour matrix" and the contour plot of the input nanoindentation quantity. The contour matrix is a single two-row matrix containing the levels and its corresponding vertices (Fig. 9).

The contour fraction is computed from:

$$C_F = \frac{L_C}{L} \tag{13}$$

where L_C is the number of contour lines belonging to the same level, and L is the total number of contour lines in the contour matrix.

To compute the phase fractions, only the contour lines corresponding to the peak values observed in the plot of levels versus C_F are considered. Then each phase fraction is given by:

$$S_F = \frac{A_c}{A_T} \tag{14}$$

where A_c is the sum of the areas associated to a peak value in the plot of levels versus C_F, and A_T is the sum of all areas associated to the peak values in the plot of levels versus C_F. A given nanoindentation quantity expressed by a contour plot can be homogenized through:

$$\psi = \sum CA_L \tag{15}$$

where C is the vector containing the levels and A_L is the vector containing the sum of the areas associated to each level.

The nanoindentation grids were analyzed in an incremental method. The minimum contour plot that can be generated by the Matlab contour function is from a 2×2 matrix. Therefore the analysis started from the second row of the nanoindentation grid, and was then incremented successively row by row until it covered the entire nanoindentation grid. At each increment, the resulting contour plot associated with a given indentation quantity was analyzed. The analysis was performed using a fixed number of contours each time. The evolution of the contour fractions was tracked by the coefficient of determination expressed by:

$$R^2 = 1 - \frac{\sum (C_{Fa} - C_{Fb})^2}{\sum \left(C_{Fa} - \overline{C_{Fa}}\right)^2} \tag{16}$$

where C_{Fa} is the vector of contour fractions in the current contour plot, C_{Fb} is the vector of contour fractions in the previous contour plot and $\overline{C_{Fa}}$ is the mean of C_{Fa}.

The logic behind the use of R^2 applied to tracking the evolution of the contour fractions, is that more than two nanoindentations produce an interval for a given nanoindentation quantity. The values on such interval are distributed on the fixed number of contours. Changes in the interval introduce changes in the sub-intervals represented by the contours. As the number of nanoindentation tests increases, the variations in the interval decrease, i.e. the representative volume element (RVE) is reached. In consequence, the value associated with each contour has small variations from the previous to the current contour plot, producing a $R^2 \approx 1$.

Finally, $R^2 \geq 0.99$ was considered as the saturation point for all the nanoindentation quantities coming from the same experiment, i.e. the point where the full range of mechanical properties of the indented surface is captured. Since R^2 has a dimensionless value, the observed nanoindentation quantities were compared and tracked along the study.

2.5. Nanoindentation inverse analysis

A computational procedure was developed to perform the elastoplastic parameter identification [24]. The routine was built using the Levenberg-Marquardt algorithm [25,26]. This algorithm requires: the definition of the objective function, the experimental nanoindentation data and the simulated nanoindentation data. These simulated data were generated numerically by a finite element model of nanoindentation test. The identification routine consists of: a) a simulation is launched with an initial set of parameters, b) the discrepancy between the experimental and numerical data is computed, c) if the discrepancy meets a given condition, the routine is finished; if not, a new simulation is launched with a new set of parameters. The condition to finish the routine is reached when the objective function has taken a value of 0.02.

2.5.1. Objective function formulation

The formulation of the objective function was based on the use of quantities obtained only from the $P - h$ curve. The total indentation work, W_t, was used to formulate the first component of the objective function through:

$$f_t = \left\| \frac{W_{t\_n} - W_{t\_e}}{W_{t\_e}} \right\| \tag{17}$$

where W_{t_e} and W_{t_n} denote the experimental and the simulated total indentation work respectively.

The elastic indentation work was used to formulate the second component of the objective function given by:

$$f_e = \left\| \frac{W_{e\_n} - W_{e\_e}}{W_{e\_e}} \right\| \tag{18}$$

where W_{e_e} and W_{e_n} denote the experimental and the simulated elastic indentation work respectively.

The third component of the objective function was obtained from:

$$f_p = \left\| \frac{P_{m\_n} - P_{m\_e}}{P_{m\_e}} \right\| \tag{19}$$

where P_{m_e} and P_{m_n} denote the experimental and the simulated maximum indentation load respectively.

The final form of the objective function was:

$$\underset{min}{f_q(\beta)} = \begin{bmatrix} f_t \\ f_e \\ f_p \end{bmatrix} \tag{20}$$

where β represents the set of sought parameters.

2.5.2. Finite element nanoindentation modeling

The nanoindentation test was simulated as an axisymmetric finite element model (Fig. 10) in Abaqus using a large strain formulation

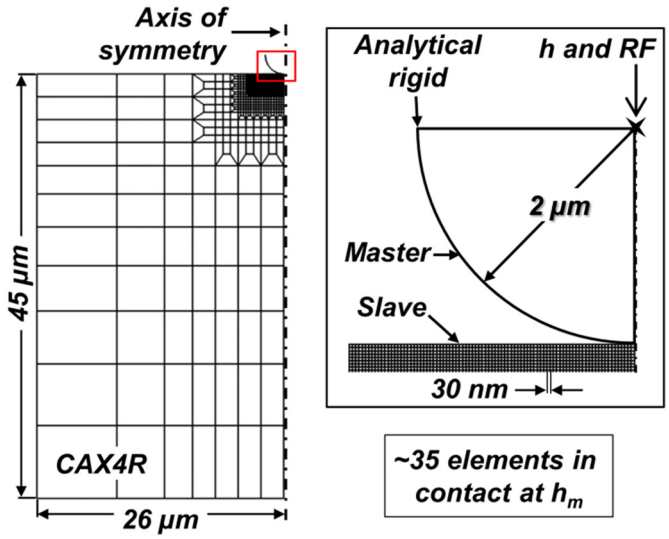

Fig. 10. Finite element model used to simulate the spherical nanoindentation.

[27]. This model results from several convergence studies. Indeed, mesh convergence, contact size and FE domain size analyses were performed by the authors in [23].

The indenter was modeled as a rigid perfect spherical indenter with a radius of 2 µm. A reference point attached to its geometry was used to impose the displacement, h, and read the reaction force, RF. The specimen was modeled as a deformable body with a minimum mesh size at the contact point of 30 nm. A mesh convergence study was conducted on the specimen to verify that the size of the model and the elements in the contact region produce results with an acceptable accuracy [23]. The bottom of the specimen was clamped. The horizontal displacement on the indenter and on the axis of symmetry of the specimen was restricted. The interaction between the indenter and the specimen was defined using the master-slave formulation with frictionless contact configuration. The plastic behavior of the specimen was modeled through Eq. (6). The elastic modulus was also used as a parameter to allow the variation on the unloading branch of the $P-h$ curve. The Poisson's ratio was $\nu = 0.3$.

3. Results

3.1. Phase fraction computing by nanoindentation grid analysis

Firstly, the nanoindentation grids conducted on the two studied materials were analyzed incrementally using 64 contour lines. The number of contours has been numerically optimized by gradually increasing it until the results stabilize. As shown in Fig. 11, both surfaces reached the saturation point after row 32 for CuZn40Pb2 brass and row 22 for W-Cu. As the trends in R^2 remained constant from a given point, it was assumed that all the mechanical properties on both surfaces were captured.

Then, using the contour fractions, C_F, the surface fractions, S_F, obtained from the contour analysis, the phase fraction corresponding to each contour level C among the studied qualities (H, E, W_e, W_t and h_m) can be determined as follows:

i. C was plotted against C_F (Fig. 12a for CuZn40Pb2 brass and Fig. 13a for W-Cu). This plot was used to determine the mean value and the standard deviation of each phase present on the indented surface. The mean value of each phase is revealed as a peak on the curve. The standard deviation corresponding to each phase was estimated from the intersections of the curve with a cutoff line coincident with the local minima found between peaks.
ii. C was plotted against S_F (Fig. 12b for CuZn40Pb2 brass and Fig. 13b for W-Cu). From this curve, the values of the surface fractions corresponding to the levels of each peak detected in C vs C_F were collected.
iii. The relative fractions, S_r, corresponding to each phase were computed from the collected surface fractions.

Finally, Table 2 summarizes the results of the contour analysis applied to the nanoindentation grids. The computed surface fractions were considered to be comparable to the phase fractions measured by EBSD particularly in the case of h_m (Table 1).

It was observed in both materials and in all nanoindentation quantities, that the calculated homogenized values, ψ, are close to the local minima between the peaks in the contour fractions plot. The relative fractions on CuZn40Pb2 brass remained coherent for all the nanoindentation quantities. For the maximum depth and the total indentation work the fractions are α~70 % , β' ~30%, while for the elastic modulus and the elastic indentation work the fractions are α~60 % , β' ~40%, exhibiting a difference of 10%. In the case of W-Cu alloy, the relative fractions for W_e, h_m and W_t, are Cu~47 % , W~52%. However for the elastic modulus the relative fractions are Cu~80 % , W~19% which are not consistent with the results given by the other nanoindentation quantities.

3.2. Inverse analysis

The homogenized values, ψ, and the mean nanoindentation quantities of the phases were used to assemble the objective functions needed

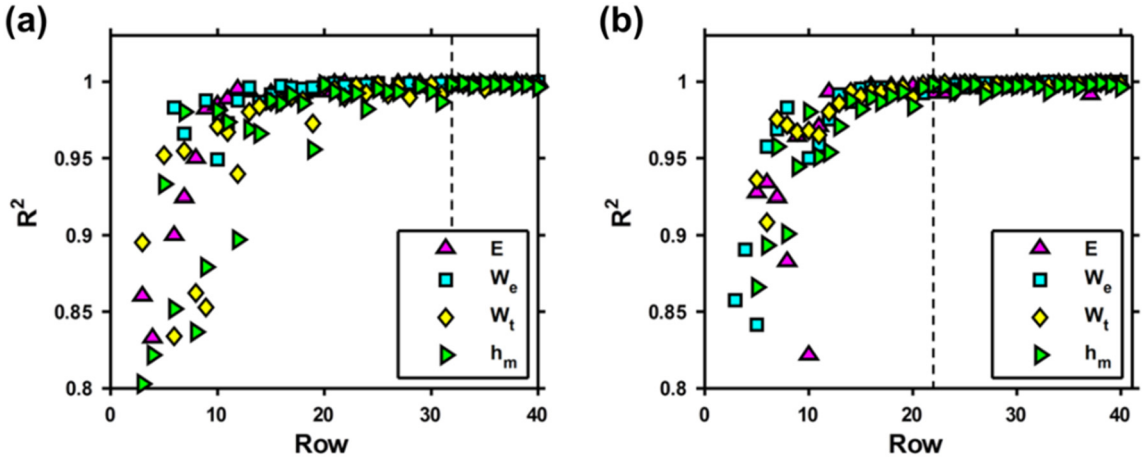

Fig. 11. Tracking of R^2 in the incremental analysis of the nanoindentation grid: (a) CuZn40Pb2 brass and (b) W-Cu.

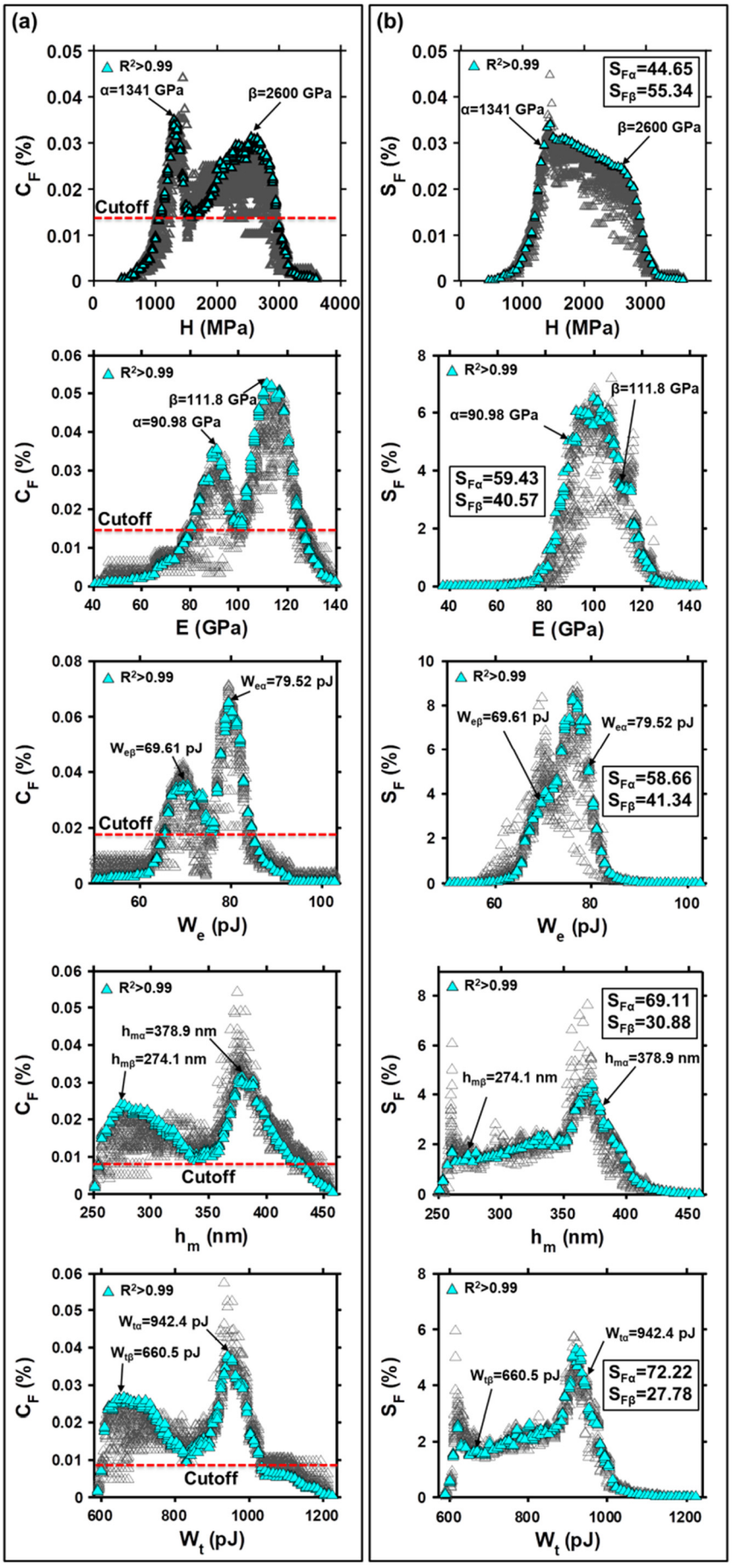

Fig. 12. Incremental analysis of nanoindentation grid applied to the surface of CuZn40Pb2 brass: (a) nanoindentation quantities versus contour fraction and (b) nanoindentation quantities versus surface fraction.

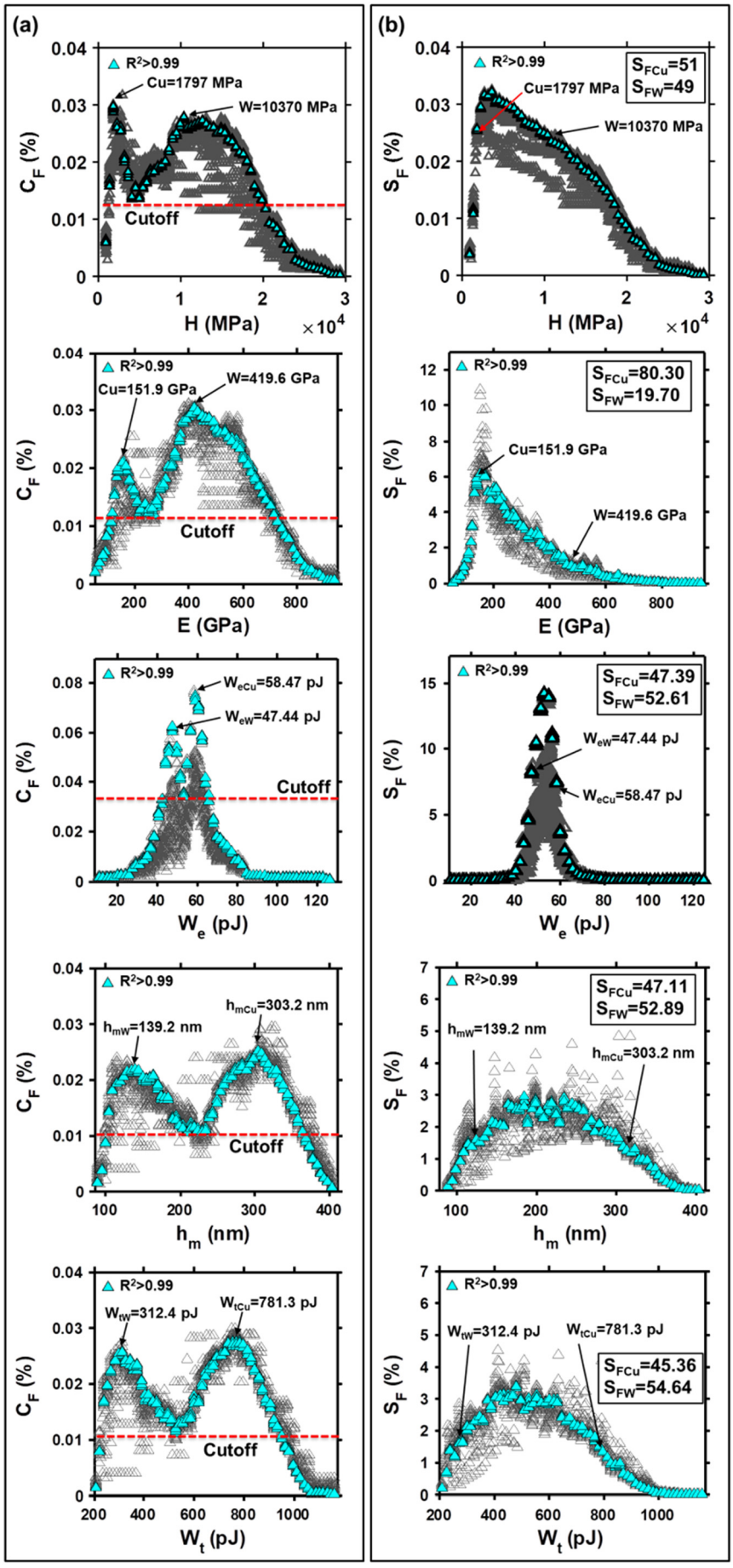

Fig. 13. Incremental analysis of nanoindentation grid applied to the surface of W-Cu: (a) nanoindentation quantities versus contour fraction and (b) nanoindentation quantities versus surface fraction.

Table 2
Results of the contour analysis applied to the nanoindentation grids.

Indented material	Nanoindentation quantity	ψ	Phase	Mean	Std	S_F (%)
CuZn40Pb2 brass	E (GPa)	101	α	91	10	59.4
			β'	112	12	40.6
	H (MPa)	1525	α	1341	257	44.7
			β'	2600	341	55.3
	W_e (pJ)	75	α	80	4	58.7
			β'	70	5	41.3
	h_m (nm)	341	α	379	44	69.1
			β'	274	43	30.9
	W_t (pJ)	835	α	942	99	72.2
			β'	661	115	27.8
W-Cu	E (GPa)	279	Cu	152	49	80.3
			W	420	222	19.7
	H (MPa)	4954	Cu	1797	451	61.1
			W	10,370	9000	38.9
	W_e (pJ)	53	Cu	58	6	47.4
			W	47	6	52.6
	h_m (nm)	220	Cu	303	67	47.1
			W	139	65	52.9
	W_t (pJ)	538	Cu	781	204	45.4
			W	312	151	54.6

to estimate the plastic parameters of the equivalent homogeneous material, and of its phases.

For CuZn40Pb2 brass, the elastoplastic parameters were determined from tensile test. The values of σ_y and n were used as reference to evaluate the accuracy of the inverse analysis (Fig. 14a, b).

The identified parameters of CuZn40Pb2 brass exhibit different values of σ_y and n for each phase. The values of the $\alpha - Phase$ are inferior to the values of the $\beta' - Phase$. The σ_y and n obtained from the homogenized nanoindentation quantities have an error of 11.4% and 2.9% with respect to the values obtained by tensile test.

The elastoplastic behavior of W-Cu used in the experiments is unknown; however the values of the yield strength of Cu and W do not match typical values ($\sigma_y = 60$ MPa for Cu, and $\sigma_y = 750$ MPa for W [28]). The σ_y of Cu was overestimated with $err = 300\%$. For W, σ_y was underestimated with $err = 53.3\%$. The hardening exponents of Cu and W were not found in the literature, so it is impossible to assess the accuracy of the estimate.

4. Discussion

Firstly, the homogenized values of the elastic modulus obtained with the contour analysis were $E = 101$ GPa for CuZn40Pb2 brass and $E = 279$ GPa for W-Cu. The homogenization technique provided in [5,7] produced the same value of the elastic modulus for CuZn40Pb2 brass, and for W-Cu, $E = 248$ GPa. Taking as a reference this value, the error on the estimate performed with the contour analysis is $err = 12.5\%$, which is an acceptable accuracy.

Then, Table 3 summarizes the surface fractions for each nanoindentation quantity computed using the statistical analysis proposed in [5,7] and the proposed method based on contour analysis. Comparing the results with the phase fractions obtained by EBSD measurements, the contour analysis produced better estimates than the statistical analysis, except for the elastic modulus and the hardness. Excluding the elastic modulus and hardness in both analyses, $err \in [9,92]\%$ for the statistical analysis and $err \in [5,36]\%$ for the contour analysis; the interval of the statistical analysis is ~2.7 times the interval of the contour analysis.

Finally, the comparison between the phase fraction estimation by the proposed method and by the EBSD analysis shows a great variability. These differences are explained by the spatial resolution of the two analysis methods. In fact, the EBSD analysis step is much smaller than the spacing between two indents. This spacing cannot be reduced to avoid interference between the deformed areas. The error of the proposed method becomes more important when the two studied phases have two very different grain sizes. In this case, unlike EBSD analysis, the gird analysis method will give a bad approximation of the small phase.

It was found that the surface fractions estimated with the elastic modulus of the W-Cu are not consistent with the rest of the nanoindentation quantities, nor with the EBSD measurements. On the other hand it was observed on the plot of C_F vs E, that the prominent peaks were coincident with the values of the phases. Therefore a "peak analysis" was conducted, i.e. the local maxima on the curve of C_F vs E, were analyzed. For CuZn40Pb2 brass only two peaks were detected: at $E = 90.98$ GPa and $E = 111.8$ GPa, therefore these two values were confirmed as the characteristic values of each phase.

In the case of W-Cu, five characteristic values were detected through the same procedure. The first peak was found at $E = 152$ GPa, with a $S_r = 48.6\%$, which is a fraction value consistent with the other indentation quantities as well as the EBSD measurements. The second peak was found at $E = 236$ GPa with a $S_r = 34.1\%$, which is a remarkable relative surface fraction. This value of the elastic modulus seems to be a mixture of the elastic properties of Cu and W. The microstructure of the W-Cu has particles of W of small size sprinkled everywhere, increasing the probability of indenting both materials at the same time (Fig. 15). On the other hand, even when both phases are fully distinguishable and the surface occupied by the Cu seems to be enough, it is not possible to determine if W is acting as a substrate on the indentations applied

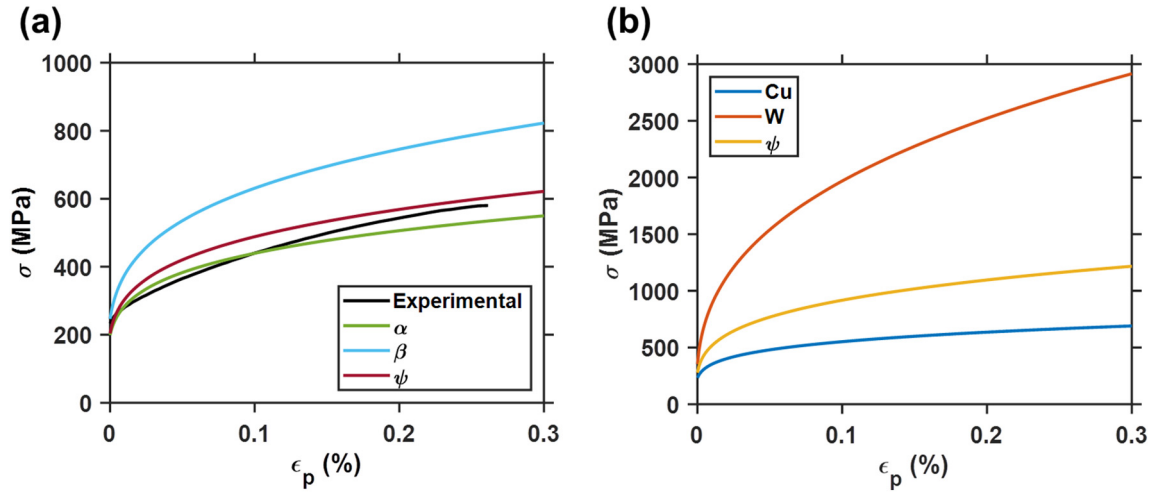

Fig. 14. Strain-stress curves determined by inverse analysis for (a) CuZn40Pb2 brass and (b) W-Cu.

Table 3
Comparison of the surface fractions obtained by statistical analysis and contour analysis with the phase fractions measured by EBSD.

Indented material	Nanoindentation quantity	Phase	Statistical analysis		Contour analysis	
			F (%)	%err (EBSD)	S_F (%)	%err (EBSD)
CuZn40Pb2 brass	E (GPa)	α	56	11	59	5
		β'	44	33	41	23
	H (MPa)	α	61	12.9	45	36
		β'	39	18.2	55	67
	W_e (pJ)	α	94	50	59	6
		β'	6	82	41	25
	h_m (nm)	α	70	12	69	10
		β'	30	9	31	6
	W_t (pJ)	α	73	16	72	15
		β'	27	18	28	16
W-Cu	E (GPa)	Cu	54	31	80	94
		W	46	15	20	51
	H (MPa)	Cu	53	6	61	22
		W	47	6	39	22
	W_e (pJ)	Cu	23	44	47	15
		W	77	92	53	31
	h_m (nm)	Cu	72	74	47	14
		W	28	30	53	32
	W_t (pJ)	Cu	78	89	45	10
		W	22	45	55	36

in Cu, what could explain why its associated elastic modulus ($E = 152$ GPa) is 1.2 times the value found in the literature [29].

The next peak was found at $E = 420$ GPa, which is consistent with the typical value of the elastic modulus of W [28]. Its relative surface fraction was $S_r = 11.9\%$, which means that this relative portion of the surface was tested in ideal conditions, i.e. without interferences from the edges of the particle or the substrate. The last peak was $E = 550$ GPa, occupying a relative surface fraction $S_r = 5.4\%$. This value of the elastic modulus is not physically justified. This is an error probably caused by identifications at the interface between the two phases. To avoid this error, the indents at the joints between the two phases must be excluded.

The phase detection performed with the statistical analysis produced good estimates of the fractions; however, it is not sensitive to the mixtures that can occur in complex materials, hiding important information about the distribution of the mechanical properties in the aggregate.

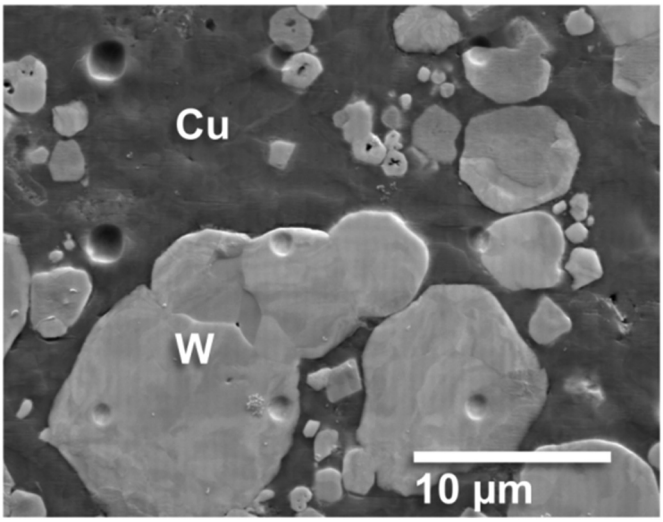

Fig. 15. SEM of an indented zone on W-Cu.

Table 4 summarizes the comparison between the mean and the standard deviation of the indentation quantities computed with the statistical analysis and the contour analysis.

The estimates of the mean values of the nanoindentation quantities performed with the statistical analysis and the contour analysis are virtually equivalent on CuZn40Pb2 brass. However on W-Cu, the statistical analysis produced an overestimated elastic modulus in both phases. In contrast, the contour analysis produced estimates of the elastic modulus that are closer to the typical values. The mean value of the rest of nanoindentation quantities is relatively close. They can be considered as equivalent.

On the other hand, the estimate of the standard deviation is similar in most cases, except for $h_m(\beta')$ and $W_t(\beta')$ on CuZn40Pb2 brass, and for $h_m(W)$ and $W_t(W)$ on W-Cu. That could be related to the skewed shape of the curves of C_F vs h_m and C_F vs W_t of both materials. However with the available data it is not possible to determine the origin of this difference.

Comparing the histograms built from the experimental nanoindentation data with the plot of the contour fraction (Fig. 16), it is evident that the histograms provide an overview of the mechanical properties, while the contour fractions provide a direct access to the relevant mechanical properties revealed as peaks in the curve.

This feature is a key point of the contour analysis, because it facilitates the interpretation of the data gathered by the nanoindentation grid.

Finally, the proposed gird analysis method makes it possible to determine with precision the value of different indentation variables relating to each phase (compared to the statistical method proposed by Randall et al. [7]), which can be used to determine different properties of each phase (e.g. elastic behavior, hardness, plastic behavior, …). It also makes it possible to determine the homogenized behavior of the material. Unlike the statistical method which requires the use of an analytical homogenization model to access this homogenized behavior so it is limited to the linear elastic behavior of the material.

4.1. Inverse analysis of nanoindentation quantities

The inverse analysis of the nanoindentation data is typically performed using the nanoindentation $P - h$ curve on a least-squares formulation [30]. The limitation of this approach is that only one curve can be analyzed each time. Other approaches allow the use of several curves at the same time in a multi-objective optimization algorithm [31]. On large quantities of indentations, these approaches can take a huge amount of simulation time, making them impractical.

The formulation of the objective function proposed in this paper effectively solves this problem because it is based on the use of the indentation quantities, which can be obtained from large groups of indentations. In combination with the contour analysis it is possible to analyze each single phase, but also to estimate the macroscopic behavior through the inverse analysis of the homogenized nanoindentation quantities.

From the tensile curve (Fig. 4), it can be stated that the increase of σ_y represents an increase of the strength of the material. The increase in the value of n introduces an increase in the strength of the material after the yielding point.

On CuZn40Pb2 brass, the pair σ_y and n corresponding to the $\alpha - Phase$ described a softer material than the pair representing the $\beta' - Phase$, which is consistent with the nanoindentation experiments, e.g. $h_m(\alpha) > h_m(\beta')$ and with the measured elasticity.

On the other hand, the pair σ_y and n obtained through the homogenized nanoindentation quantities matches the tensile test with great accuracy, especially for n, demonstrating that the proposed formulation of the objective function can deal with a large number of nanoindentations.

However, in the case of W-Cu, even when the tensile properties are unknown, the effects of the complex microstructure are evident. For example the yield strength of Cu is overestimated, meaning that

Table 4
Contrast of the mean and standard deviation of the indentation quantities estimated through statistical analysis and contour analysis.

Indented material	Nanoindentation quantity	Phase	Statistical analysis		Contour analysis			
			Mean	Std	Mean	*%err*	Std	*%err*
CuZn40Pb2 brass	E (GPa)	α	93	8	91	2	10	25
		β'	114	9	112	2	12	33
	H (MPa)	α	1339	145	1341	0.5	257	77
		β'	2536	442	2600	2.5	341	23
	W_e (pJ)	α	75	6	80	7	4	33
		β'	72	11	70	3	5	55
	h_m (nm)	α	374	30	379	1	44	47
		β'	269	14	274	2	43	207
	W_t (pJ)	α	916	94	942	3	99	5
		β'	627	23	661	5	115	400
W-Cu	E (GPa)	Cu	170	43	152	11	49	14
		W	452	190	420	7	222	17
	H (MPa)	Cu	2367	992	1797	24	451	75
		W	11,890	6427	10,370	12.8	9000	40
	W_e (pJ)	Cu	56	14	58	4	6	57
		W	53	6	47	11	6	0
	h_m (nm)	Cu	265	75	303	14	67	11
		W	118	19	139	18	65	242
	W_t (pJ)	Cu	632	215	781	24	204	5
		W	256	35	312	22	151	331

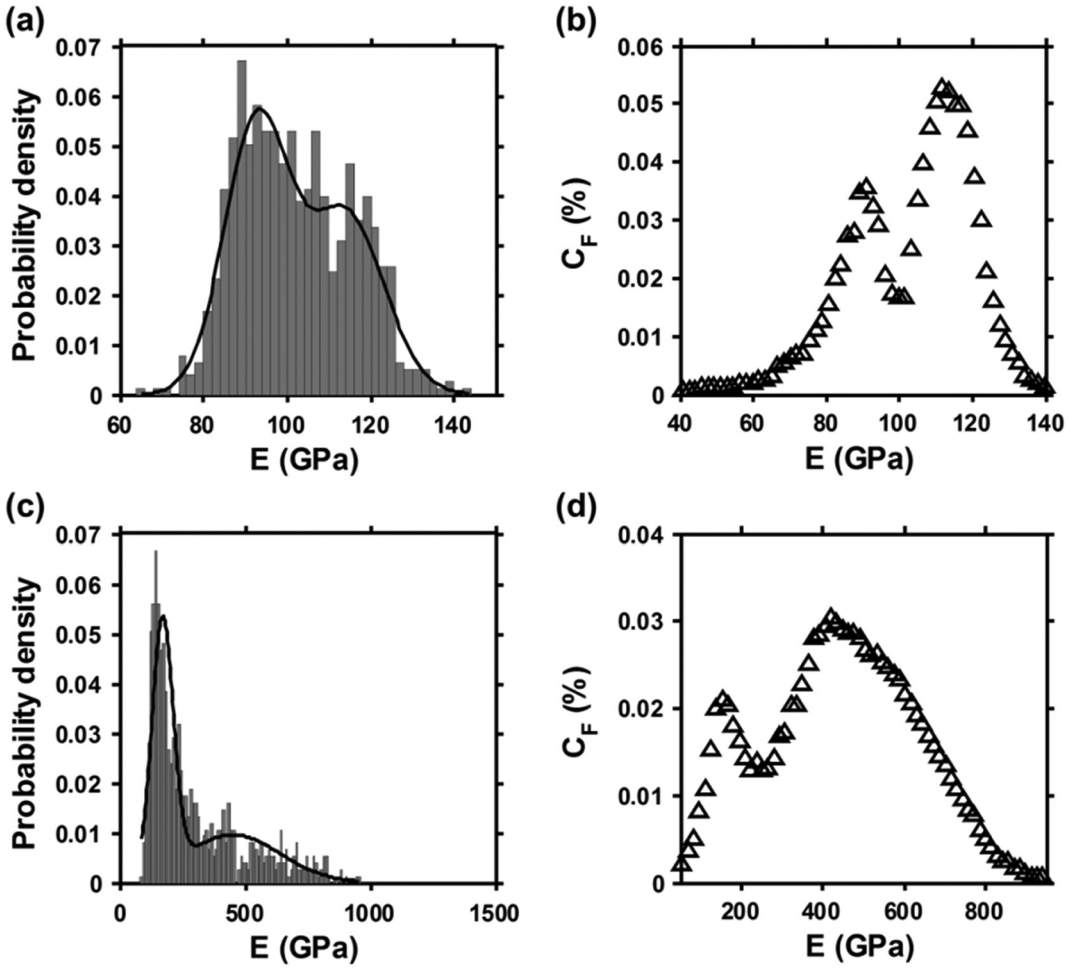

Fig. 16. Comparison between the statistical analysis and the contour analysis applied to the elastic modulus: (a) histogram and (b) contour analysis of CuZn40Pb2 brass; (c) histogram and (d) contour analysis W-Cu.

W interfered in the estimation. The yield strength of W was underestimated, revealing the influence of Cu. The value of the hardening exponent of W and Cu is unknown; therefore it is not possible to know if there was interference between them.

4.2. Validity of the nanoindentation grid method

According to [5,7], the nanoindentation grid must satisfy a set of specific characteristics to be able to assess with good accuracy the

mechanical properties of each phase in the heterogeneous material. To measure individually the mechanical properties of each phase, the characteristic diameter, D, of a particle in the heterogeneous material must be $h \ll D$, at most $h < 0.1D$. This proportion was estimated for Berkovich indentation. The applicability of this rule to the spherical indenter used in the experiments can be explained through the comparison of the diameter of the projected area in function of h. The Berkovich indenter can be represented as a conical indenter with an apex angle $\theta = 70.3°$ [20,32]. The diameter of the projected circle at given h is computed from the expression:

$$d_B = 2\tan(\theta)h \tag{21}$$

The diameter of the projected circle at given h of the spherical indenter, is obtained with [33]:

$$d_s = 2\sqrt{2Rh - h^2} \tag{22}$$

where R is the radius of the indenter.

The computed values of d_B and d_s are based on the assumption of ideal contact with the surface of the sample, i.e. free of pile-up or sinking-in [32].

By plotting d_B and d_s versus h (Fig. 17), a linear growth of the diameter of the Berkovich indenter is observed, revealing its homothetic nature. On the spherical indenter an asymptote is observed for a diameter of 4 μm, which is the limit of the ideal sphere of $R = 2$ μm.

During nanoindentation experiments, the nanoindentation depth in CuZn40Pb2 brass was $h_m \in [248,460]$ nm and $h_m \in [85,406]$ nm in W-Cu. The maximum depths reached on both materials are close to the diameter shared by the spherical indenter and the Berkovich indenter, therefore the rule relating the diameter of the particle and the nanoindentation depth can be applied directly to the spherical indenter used in the experiments.

In the case of the CuZn40Pb2 brass, considering the mean diameter of the particle determined by EBSD measurements and the maximum reached depth, $h/D = 0.024$. The worst scenario is when the maximum depth is reached in the smallest particle, which has a diameter of 7.81 μm (Fig. 3a), then $h/D = 0.059$. Therefore in both cases it is expected that the selected loading force of 5 mN gives access to the mechanical properties of each phase without interferences.

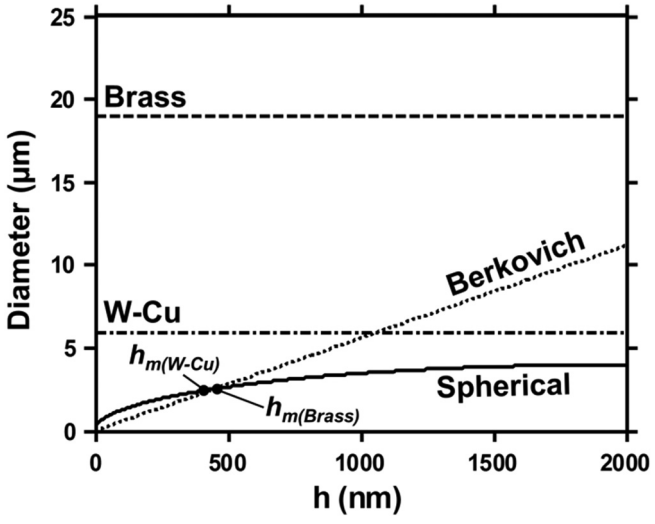

Fig. 17. Comparison of the diameters of the projected circles for a Berkovich indenter (equivalent cone), and the spherical indenter as a function of the nanoindentation depth. The mean diameters of the particles in CuZn40Pb2 brass and W-Cu are also presented.

In the case of the W-Cu, $h/D = 0.069$. In the worst scenario, the particle has a diameter of 2.94 μm (Fig. 3b), with $h/D = 0.138$, therefore interference on the measurements between the phases can occur.

The maximum diameter of the residual imprint in both materials was ~2.5 μm, therefore the selected grid spacing of 10 μm was enough to avoid interferences between tests.

Finally, the size of the nanoindentation grid must satisfy $d_i\sqrt{N} \gg D$, where d_i is the distance between indentations and N is the number of indentations. Considering the grid conducted on each sample (800 indentations with grid spacing of 10 μm), $D/\left(d_i\sqrt{N}\right)$, produces 0.067 for CuZn40Pb2 brass and 0.021 for W-Cu alloy. Therefore the size of the grid applied on CuZn40Pb2 brass was enough to be representative of the bulk; however in W-Cu the grid had an overestimated size. These two conditions were confirmed in the Fig. 11, where the minimum required grid for CuZn40Pb2 brass was 20 × 32, and 20 × 22 for W-Cu. For these grids $D/\left(d_i\sqrt{N}\right)$ produces 0.075 and 0.028 for CuZn40Pb2 brass and W-Cu respectively.

5. Conclusion

First of all, the nanoindentation grid is a powerful method giving access to the mechanical properties of phases existing at the microscale. The contour analysis proposed in this paper is a perfect complement to nanoindentation grid: 1) it is able to determine whether the nanoindentation grid captured all the mechanical properties. 2) it gives access to the mean value of the phases and also to the macroscopic behavior from a single plot. 3) it estimates the phase fractions of simple microstructures with an improved accuracy. 4) for complex microstructures, it gives access to the spectrum of mechanical properties, facilitating the interpretation and the understanding of the mechanical behavior. In this case, the analysis of all the nanoindentation quantities gives the contrast necessary to determine the correct value of the phase fractions. 5) the standard deviation can be estimated. However for some nanoindentation quantities its value can depend on the type of distribution. More studies need to be performed to have a clear understanding on the estimation of the standard deviation by contour analysis.

Then, the provided formulation of the inverse analysis demonstrated a great accuracy and capacity to deal with large amounts of nanoindentation.

Generally, the pdf provides more information on the statistical distribution of a variable compared to the cdf. In the literature, the cdf is often used because the pdf is highly sensitive to the choice of the bin size e.g. in the work proposed by Randall et al. [7], the authors have chosen to use the cdf. The advantage of the method based on gird analysis is that the bin size is defined directly following the choice of the number of iso-contours. This number has already been optimized before (64 iso-contours).

Finally, the combination of the nanoindentation grid, the contour analysis and the inverse analysis provides a powerful tool for the characterization of elastoplastic materials from simple to complex microstructures. The implementation of the contour analysis on the software controlling the nanoindenter could help to automate the characterization process eliminating waste by performing only the needed amount of tests, making the nanoindenter a true surface scanner.

The use of indentation tests at constant maximum load for the two phases constitutes a strong hypothesis of this study because the mechanical behavior of the two phases is characterized at two different strain levels. A way of improving this method is to adapt the load to have equivalent strain levels. It is also possible to explore the non-homothetic property of the spherical tip geometry by performing cyclic indentations.

CRediT authorship contribution statement

Cesar-Moises Sanchez-Camargo: Methodology, Formal analysis, Investigation, Writing - original draft. **Anis Hor:** Conceptualization, Methodology, Writing - review & editing. **Mehdi Salem:** Resources, Validation, Writing - review & editing. **Catherine Mabru:** Conceptualization, Writing - review & editing, Supervision.

Declaration of competing interest

The authors declare that they have no known competing financial interests or personal relationships that could have appeared to influence the work reported in this paper.

Acknowledgments

This work was partially supported by the Mexican Council of Science and Technology (CONACYT). We wish to acknowledge the assistance of Mr. Thierry Martin for the optimum performance of the nanoindenter. The assistance of Dr. Victor Sanchez in the review of this manuscript is gratefully acknowledged. We wish also to acknowledge all the ISAE-SUPAERO DMSM team.

References

[1] W.C. Oliver, G.M. Pharr, An improved technique for determining hardness and elastic modulus using load and displacement sensing indentation experiments, J. Mater. Res. 7 (1992) 1564–1583.
[2] W.C. Oliver, G.M. Pharr, Measurement of hardness and elastic modulus by instrumented indentation: advances in understanding and refinements to methodology, J. Mater. Res. 19 (1) (2004) 3–20.
[3] I.N. Sneddon, The relation between load and penetration in the axisymmetric Boussinesq problem for a punch of arbitrary profile, Int. J. Eng. Sci. 3 (%11) (1965) 47–57.
[4] K.L. Johnson, Contact Mechanics, Cambridge University Press, 1987.
[5] G. Constantinides, K. Ravi Chandran, F.-J. Ulm, K. Van Vliet, Grid indentation analysis of composite microstructure and mechanics: principles and validation, Mater. Sci. Eng. A 430 (%11) (2006) 189–202.
[6] P.S. Phani, W. Oliver, A critical assessment of the effect of indentation spacing on the measurement of hardness and modulus using instrumented indentation testing, Mater. Des. 164 (2019) 107563.
[7] N.X. Randall, M. Vandamme, F.-J. Ulm, Nanoindentation analysis as a two-dimensional tool for mapping the mechanical properties of complex surfaces, J. Mater. Res. 24 (%13) (2009) 679–690.
[8] L. Brown, P.G. Allison, F. Sanchez, Use of nanoindentation phase characterization and homogenization to estimate the elastic modulus of heterogeneously decalcified cement pastes, Mater. Des. 142 (2018) 308–318.
[9] M. Sebastiania, R. Moscatellia, F. Ridib, P. Baglionib, C. F., High-resolution high-speed nanoindentation mapping of cement pastes: unravelling the effect of microstructure on the mechanical properties of hydrated phases, Mater. Des. 97 (2016) 372–380.
[10] B. Vignesh, W. Oliver, G. Siva Kumar, P. Sudharshan Phani, Critical assessment of high speed nanoindentation mapping technique and data deconvolution on thermal barrier coatings, Mater. Des. 181 (2019) 108084.
[11] E. Ariza-Echeverri, Masoumi, A. Nishikawa, D. Mesa, A. Marquez-Rossy, A. Tschiptschin, Development of a new generation of quench and partitioning steels: influence of processing parameters on texture, nanoindentation, and mechanical properties, Mater. Des. 186 (%1108329) (2020).
[12] X. Zhu, Y. Yuan, L. Li, Y. Du, F. Li, Identification of interfacial transition zone in asphalt concrete based on nano-scale metrology techniques, Mater. Des. 129 (2017) 91–102.
[13] C. Singh, J. Singh, Accurate contour plotting using 6-node triangular elements in 2d, Finite Elem. Anal. Des. 45 (%12) (2009) 81–93.
[14] A. Ruiz-Moreno, P. Hähner, Indentation size effects of ferritic/martensitic steels: a comparative experimental and modelling study, Mater. Des. 145 (2018) 168–180.
[15] M. Ghidelli, M. Sebastiani, C. Collet, R. Guillemet, Determination of the elastic moduli and residual stresses of freestanding Au-TiW bilayer thin films by nanoindentation, Mater. Des. 106 (2016) 436–445.
[16] A. Elsayed, W. Li, O.A. El Kady, W.M. Daoush, E.A. Olevsky, R.M. German, Experimental investigations on the synthesis of W-Cu nanocomposite through spark plasma sintering, J. Alloys Compd. 639 (2015) 373–380.
[17] F. Bachmann, R. Hielscher, H. Schaeben, Grain detection from 2d and 3d EBSD data—specification of the MTEX algorithm, Ultramicroscopy 111 (%112) (2011) 1720–1733.
[18] F. Bachmann, R. Hielscher, P.E. Jupp, W. Pantleon, H. Schaeben, E. Wegert, Inferential statistics of EBSD data from within individual crystalline grains, J. Appl. Crystallogr. 43 (2010) 1338–1355.
[19] J.R. Davis, Tensile Testing, ASM International, 2004.
[20] M. Dao, N.V. Chollacoop, K.J. Van Vliet, T.A. Venkatesh, S. Suresh, Computational modeling of the forward and reverse problems in instrumented sharp indentation, Acta Mater. 49 (2001) 3899–3918.
[21] H. Pelletier, J. Krier, A. Cornet, P. Mille, Limits of using bilinear stress–strain curve for finite element modeling of nanoindentation response on bulk materials, Thin Solid Films 379 (2000) 147–155.
[22] C.-M. Sanchez-Camargo, A. Hor, C. Mabru, A robust inverse analysis method for elastoplastic behavior identification using the true geometry modeling of Berkovich indenter, Int. J. Mech. Sci. 171 (2020) 105370.
[23] C.-M. Sanchez-Camargo, Mechanical Multi-scale Characterization of Metallic Materials by Nanoindentationtest, (PhD Thesis) Toulouse University, 2019.
[24] G. Konstantopoulos, E.P. Koumoulos, C.A. Charitidis, Classification of mechanism of reinforcement in the fiber-matrix interface: application of machine learning on nanoindentation data, Mater. Des. 192 (2020) 108705.
[25] E. Lee, Theory of Electrophoresis and Diffusiphoresis of Highly Charged Colloidal Particles, Academic Press, 2018.
[26] E. Rolfe, M. Kelly, H. Arora, J. Dear, Composite materials for blast applications in air and underwater, Dyn. Response Fail. Compos. Mater. Struct. (2017) 263–295.
[27] V. Buljak, Inverse Analyses With Model Reduction: Proper Orthogonal Decomposition in Structural Mechanics, Springer Science & Business Media, 2011.
[28] D.W. Marquardt, An algorithm for least-squares estimation of nonlinear parameters, J. Soc. Ind. Appl. Math. 11 (%12) (1963) 431–441.
[29] M.K. Transtrum, B.B. Machta, J.P. Sethna, Geometry of nonlinear least squares with applications to sloppy models and optimization, Phys. Rev. E 83 (%113) (2011) 36701.
[30] P.L. Larsson, A.E. Giannakopoulos, E. Söderlund, D.J. Rowcliffe, R. Vestergaard, Analysis of Berkovich indentation, Int. J. Solids Struct. 33 (%12) (1996) 221–248.
[31] M.F. Ashby, D.R.H. Jones, Engineering Materials 1: An Introduction to Properties, Applications and Design, 2012.
[32] A.B. Lebedev, Y.A. Burenkov, A. Romanov, V.I. Kopylov, V.P. Filonenko, V. Gryaznov, Softening of the elastic modulus in submicrocrystalline copper, Mater. Sci. Eng. A 203 (%11–2) (1995) 165–170.
[33] J.-M. Collin, G. Mauvoisin, P. Pilvin, Materials characterization by instrumented indentation using two different approaches, Mater. Des. 31 (%11) (2010) 636–640.